

Blueshifting the Onset of Optical UV Absorption for Water under Pressure

Andreas Hermann*

*Department of Chemistry, The University of Auckland, Private Bag 92019, Auckland, New Zealand
MacDiarmid Institute for Advanced Materials and Nanotechnology, School of Chemical and Physical Sciences,
Victoria University Wellington, New Zealand*

Peter Schwerdtfeger†

*Centre for Theoretical Chemistry and Physics, The New Zealand Institute for Advanced Study, Massey University (Auckland Campus),
Private Bag 102904, North Shore City, 0745 Auckland, New Zealand*

(Received 17 January 2011; revised manuscript received 11 April 2011; published 6 May 2011)

First-principles calculations show that the optical UV absorption onset of solid water is blueshifted with increasing pressure. Across several crystal structures and a wide pressure range, the optical gap increases almost linearly with external pressure, making solid water more transparent. The origin of this unusual effect can be traced back to an increased Stark shift caused by water's electrostatic environment at smaller volumes.

DOI: 10.1103/PhysRevLett.106.187403

PACS numbers: 78.20.Ci, 71.35.Cc, 78.40.Pg

The study of materials under high pressure has become a very active research field in recent years as familiar materials often crystallize in new phases, with novel and intriguing properties [1–3]. Experimentally, advances in diamond anvil cell technology allow access to pressures up to about 400 GPa; higher pressures are found only in high-energetic detonations, comet collisions, or the interior of heavy planets. For the latter, for instance, studying pressurized solid hydrogen or ice (and its possible transition to a metallic phase) is of huge interest for planets like Jupiter or Neptune [4]. Water and ice under pressure are of particular interest for the ocean floor where ice forms clathrates [5] or in the upper mantle of our Earth [6]. Pressure-induced changes in the molecular coordination are accompanied by changes in the electronic structure of liquid water [7]. In the solid phase, the flexibility of the hydrogen bonds allows for an abundance of different crystalline structures that are stable under certain pressure and temperature regimes [8–11]. The electronic properties of solid ice under pressure are, however, currently not well understood [3,5,6].

Similarly, little is known about the optical spectrum of ice under pressure. Benoit *et al.* briefly mention in their *ab initio* molecular dynamics study of high-pressure ice phases that the electronic band gap at the density-functional theory (DFT) level increases under pressure [12]. The refractive index of ice in the visible frequency range has been measured and found to increase monotonically, up to pressures of 120 GPa [13,14]. Recently, we studied the blueshift of the optical absorption onset upon condensation of water molecules [15]: In the gas, liquid, and solid phases, water's first UV absorption peak appears at 7.4, 8.2, and 8.7 eV, respectively [16–19]. This effect has been attributed to molecular excitonic effects [20], solvation and Rydbergization effects [21], and excitonic

delocalization effects [22]. In our recent work, we were able to isolate the electrostatic field of the crystalline environment as the driving force in the anomalous blueshift of water's absorption spectrum [15]—an enormous Stark effect caused by the dipole electric field that opens the optical gap of a water molecule by more than 1 eV. Here, we study the absorption spectrum of ice under pressure from first principles and find a linear increase of the onset of absorption up to high pressures.

The thermodynamically stable ice phase under low temperature and low pressure conditions is ice XI (space group 36, $Cmc2_1$), a ferroelectric hydrogen ordered version of the hexagonal ice phase Ih found under ambient conditions. With increasing pressure, ice XI is thought to be succeeded by rhombohedral and hydrogen ordered ice II (space group 148, $R\bar{3}$), even though the actual transition ice XI \rightarrow ice II has not been verified experimentally. Ice II was recently found to be succeeded by ice XV (space group 2, $P\bar{1}$) under pressures higher than about 0.8 GPa [11]. Ice XV is a hydrogen ordered counterpart of tetragonal ice VI. Increasing pressure beyond about 1.5 GPa, antiferroelectric ice VIII (space group 141, $I4_1/amd$) is most stable, a hydrogen ordered counterpart of ice VII [23]. Experimental results show stability of ice VIII up to about 62 GPa after which ice VII (which we have not included in this study) becomes stable. This transition from an ordered to a disordered hydrogen network is explained by computational studies to be due to proton tunneling and to be followed by transitions to a hydrogen disordered ice X-like structure and finally (at about 120 GPa) to hydrogen ordered ice X (space group 224, $Pn\bar{3}m$) [24–27]. In ice X, hydrogens are placed at the midpoint of hydrogen bonds, thus marking the transition from a molecular to an atomic crystal. Post-X ice (space group 57, $Pbcm$) has been predicted from molecular dynamics

simulations to occur at pressures around 300–400 GPa [12,27], with further transitions to *Pbca* (space group 61) and *Cmcm* structures (space group 63) at pressures of 760 and 1550 GPa, respectively [28].

Different ice crystal structures were investigated at pressures up to 300 GPa, from hexagonal ice XI, the intermediate pressure modifications ice II, ice XV, and ice VIII, to the ultrahigh-pressure modification ice X, with structural parameters optimized by using DFT [29]. By utilizing a plane wave basis, the electron-ion interaction was modeled by using non-norm-conserving ultrasoft pseudopotentials [30], thus allowing a modest plane wave cutoff energy of 15 a.u. Regular k -point meshes were used to sample the Brillouin zone [31], including 6 (4; 11; 20) irreducible k points for ice XI (XV; VIII; X). Perdew and Wang's generalized gradient parametrization of the exchange-correlation energy [Perdew-Wang 1991 (PW91)] was used [32]. For all phases, unit cell parameters and internal coordinates were optimized until the remaining forces acting on the ions were smaller than 5 meV/Å. The calculations of the optical absorption spectra are based on the DFT structures and wave functions, utilizing many-body perturbation theory [33–35]: In a first step, a perturbational treatment of the electronic self-energy is used to calculate, within the G_0W_0 approximation, electronic quasiparticle energies; in a second step, the electron-hole interaction of optically excited states is included to obtain absorption spectra with excitonic and local field effects, hence solving the Bethe-Salpeter equation for the macroscopic polarization function. This approach has been used to calculate absorption spectra of water in its extended phases [15,22,36], in good agreement with experimental data [16–19]. A model dielectric function was used to evaluate the screened Coulombic interaction W , in both the G_0W_0 and the Bethe-Salpeter equation calculations [37]. Its free parameter, the high-frequency dielectric constant ϵ_0 , was adjusted to give band energies in agreement with self-consistent GW_0 calculations [38] and was found to increase from $\epsilon_0 = 2.0$ at zero pressure in ice XI to $\epsilon_0 = 4.0$ at $p = 270$ GPa in ice X; this trend is in line with experimentally determined refractive indices of ice under pressure [14]. Doubling the plane wave cutoff to 30 a.u. changed the G_0W_0 eigenvalues by less than 5 meV. For ice XI (XV; VIII; X), the Bethe-Salpeter equation was solved by using 32 (48; 64; 512) random k points.

Calculated ground state properties are listed in Table I. The geometrical parameters of all phases are well reproduced by using DFT-PW91, with a slight overestimation of the hydrogen bond strengths resulting in a systematic underestimation of lattice parameters and an overall over-binding effect. For ice XI, the binding energy is about 25% too high [45]; the rather large discrepancy for the bulk modulus of ice XI may result from finite temperature effects, as the experiment was carried out with ice Ih at about 250 K [44]. For ice VIII, the experimental bulk

TABLE I. Ground state properties of various ice phases from DFT-PW91 calculations: equilibrium lattice constants a , b , and c (Å), equilibrium volume V_0 (Å³/molecule), binding energy E_b (eV/molecule), and bulk modulus B_0 (kbar) where experimental values for the bulk modulus B_0 are missing (last column).

Phase	Level	a	b	c	V_0	E_b	B_0
XI	PW91	4.396	...	7.152	29.80	-0.719	152.5
	Expt.	4.502 ^a	...	7.328	32.15	-0.580 ^f	89.0 ^g
II	PW91	7.609 ^b	24.02	-0.650	158.7
	Expt.	7.78	25.35	...	
XV	PW91	6.025	6.033	5.630	20.46	-0.587	227.2
	Expt.	6.232 ^c	6.244	5.790	22.53	...	
VIII	PW91	4.770	...	6.965	19.81	-0.511	192.4
	Expt.	4.656 ^d	...	6.775	19.89 ^e	...	241
X	PW91	2.932	12.60	+0.268	1947.3

^aFrom Ref. [39].

^bFrom Ref. [40].

^cFrom Ref. [11] at 0.9 GPa.

^dFrom Ref. [41] at 2.4 GPa.

^eFrom Ref. [42].

^fFrom Ref. [43].

^gFrom Ref. [44].

modulus is derived from equation of state fits of experimental data, extrapolated to zero kelvin; it is smaller in our calculations. Wave-function-based coupled cluster methods within incremental schemes including zero-point vibrational effects have been shown to yield very good results for hexagonal ice Ih [45,46], and could prove more accurate for other ice phases as well, but are computationally demanding and do not provide information on the electronic band structure needed for excited state calculations.

Phase transitions under pressure are studied by comparing the Gibbs free energies $G = U + pV + TS$ for the different phases. However, in the low temperature regime, this expression is reduced to $G = U + pV$, and with the

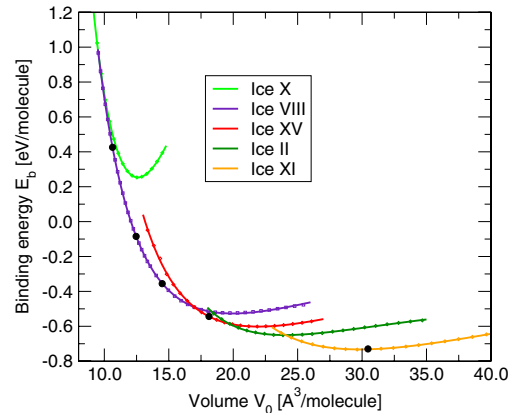


FIG. 1 (color online). Energy-volume relations for all ice phases studied here. Small symbols indicate data points, solid lines indicate equation of state fits, and black circles indicate some of the points where optical spectra were calculated.

additional neglect of zero-point vibrational effects it can be assumed that $U \approx E_b$; i.e., the free energy equals the lattice binding energy. The transitions found are in qualitative agreement with experimental findings. The transition ice XI \rightarrow ice II is found to occur at $p = 2.49$ GPa, ice II \rightarrow ice XV at $p = 4.35$ GPa, ice XV \rightarrow ice VIII at $p = 6.92$ GPa, and ice VIII \rightarrow ice X at $p = 96.4$ GPa. The last transition, as can be seen in Fig. 1, is difficult to assign to a specific transition pressure, as ice VIII's lattice energy smoothly approaches ice X's energy curve under high pressure. A transition pressure for the ice XI \rightarrow ice II transition has not been established experimentally. The stability region of ice XV, however, was assigned experimentally to the pressure range $p = 0.8 \dots 1.5$ GPa [11], whereas we find the stability range $p = 4.35 \dots 6.92$ GPa, which perhaps originates from the neglect of zero-point vibrational effects. The transition pressure of 96.4 GPa we find for the ice VIII \rightarrow ice X transition fits into the general picture of the behavior of high-pressure ice.

The absorption spectra for ices XI, XV, VIII, and X are shown in Fig. 2. All spectra, independent of the crystal structure, exhibit a prominent excitonic absorption peak. This holds true especially for the atomic crystal ice X. Figure 2 illustrates the anomalous optical behavior of ice: Under increased pressure, the optical band gap increases substantially. The intensity increases with decreasing volume as well, as one would expect from the volume behavior of the extinction coefficient. An important consequence of this behavior is that ice thus becomes more and more transparent under pressure. This trend is being followed through the transitions from ice XI to ice XV and on to ice VIII; in fact, even though the crystal structures of these phases look very different, their optical spectra share a remarkable similarity, at least at comparatively low pressures. Water in all these phases exhibits the same tetrahedral nearest neighbor environment, thus hinting at a point argued previously [15] that the local electrostatic

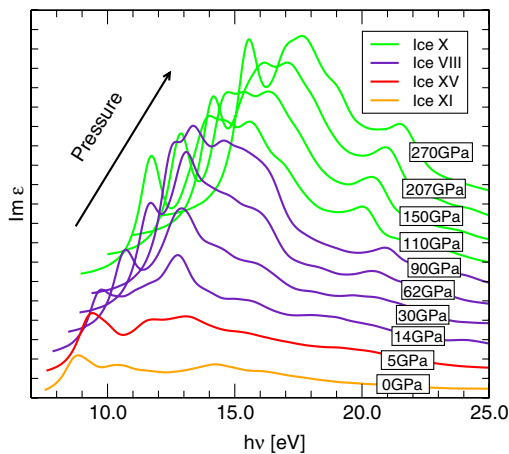


FIG. 2 (color online). Many-body optical absorption spectra of various ice crystal structures under pressure. Spectra are offset vertically for clarity.

environment of water molecules in ice determines their optical properties. Therefore, we performed a similar set of calculations for all these crystal structures, accounting for the electrostatic environment of water molecules in the solid by constructing the dipole electric field around each distinct molecule in the respective unit cell and using the symmetry-adapted cluster configuration interaction approach [47–49] to obtain optical excitation spectra, as described in Ref. [15]. We kept the dipole moment of water in ice fixed to the value of 3 D found in previous calculations [50,51] but also investigated the effect of increasing the dipole moment with pressure proportional to the dielectric constant used in the model dielectric function of the excitonic calculations. Figure 3 compares the pressure dependence of the respective first absorption peak energy of the excitonic spectra with these electric field calculations. Assuming a constant water dipole moment, we can reproduce the increase of the optical gap under pressure, however, with a much smaller slope than found in the excitonic calculations. Scaling the dipole moment with the dielectric constant leads to a systematic overestimation of the optical gap while still exhibiting a monotonic increase under pressure. While both model approaches describe the optical behavior of ice qualitatively, they do not agree as well quantitatively with the excitonic approach as under ambient conditions [15]. The increase of the molecular optical gap can be traced back to the dipole electric field's influence (an inhomogeneous Stark effect) on the molecular single-particle energy levels, especially a

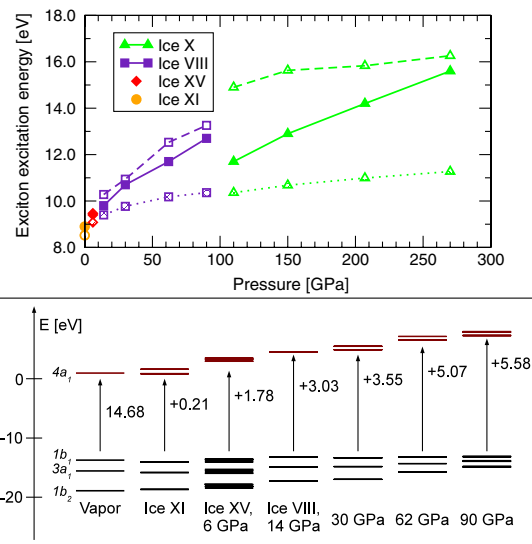


FIG. 3 (color online). Upper panel: Optical band gaps of spectra from Fig. 2 (filled symbols, solid lines) and from electric field calculations with fixed (hashed symbols, dotted lines) and scaled (open symbols, dashed lines) point charges, all plotted against external pressure. Lower panel: Occupied (black lines) and unoccupied (red lines) Hartree-Fock energy levels of water in vapor and molecular crystal structures, with a single-particle gap increase relative to vapor phase.

quenching of the lowest unoccupied $4a_1$ molecular orbital [of $\sigma^*(O-H)$ character]. Figure 3 illustrates this for the molecular ice structures. It seems clear that with increased overlap of molecular orbitals under pressure (especially in degenerate ice X) the idea of stripping down interactions in the solid to solely electrostatic effects must break down. There is a notable drop in the excitonic optical gap upon transition from ice VIII to ice X; however, with further increasing pressure, we find an almost linear increase of the optical gap up to about 15.5 eV at $p = 270$ GPa. Of course, under even higher pressures, the atomic orbital overlap will lead to much larger band dispersion and eventually closure of the electronic band gap. This metallic phase transition was proposed recently by computational studies in the transition from post-ice X phases with $Pbca$ to $Cmcm$ symmetry at $p = 1550$ GPa [28].

In conclusion, first-principles calculations show that the onset of the optical absorption of ice undergoes a blueshift with increasing pressure, thus opening up the optical gap even further compared to liquid and solid water under ambient conditions. This is consistent with molecular calculations which consider the crystalline dipole electric fields of the various ice phases. Solid water becomes more transparent under pressure, driven by an enhanced Stark effect that widens the molecular electronic gap.

Funding through the Marsden Fund (MAU0606), Education NZ, and the MacDiarmid Institute is gratefully acknowledged.

*Present address: Department of Chemistry and Chemical Biology, Cornell University, Ithaca, NY 14850, USA.
a.hermann@auckland.ac.nz

†p.a.schwerdtfeger@massey.ac.nz

- [1] J. V. Badding, *Annu. Rev. Mater. Sci.* **28**, 631 (1998).
- [2] A. Mujica *et al.*, *Rev. Mod. Phys.* **75**, 863 (2003).
- [3] W. Grochala *et al.*, *Angew. Chem., Int. Ed.* **46**, 3620 (2007).
- [4] C.J. Pickard and R.J. Needs, *Nature Phys.* **3**, 473 (2007).
- [5] E. Sloan and C. Koh, *Clathrate Hydrates of Natural Gases*, Chemical Industries (CRC Press, Boca Raton, 2008).
- [6] D. Green, *Earth Planet. Sci. Lett.* **19**, 37 (1973).
- [7] E. Schwegler, G. Galli, and F. Gygi, *Phys. Rev. Lett.* **84**, 2429 (2000).
- [8] V.F. Petrenko and R.W. Whitworth, *Physics of Ice* (Oxford University, New York, 1999).
- [9] C.G. Salzmann *et al.*, *Science* **311**, 1758 (2006).
- [10] B. Schwager and R. Boehler, *High Press. Res.* **28**, 431 (2008).
- [11] C.G. Salzmann *et al.*, *Phys. Rev. Lett.* **103**, 105701 (2009).
- [12] M. Benoit *et al.*, *Phys. Rev. Lett.* **76**, 2934 (1996).
- [13] A. Dewaele *et al.*, *Phys. Rev. B* **67**, 094112 (2003).
- [14] C.-S. Zha *et al.*, *J. Chem. Phys.* **126**, 074506 (2007).
- [15] A. Hermann, W.G. Schmidt, and P. Schwerdtfeger, *Phys. Rev. Lett.* **100**, 207403 (2008).
- [16] G.D. Kerr *et al.*, *Phys. Rev. A* **5**, 2523 (1972).
- [17] H. Hayashi *et al.*, *Proc. Natl. Acad. Sci. U.S.A.* **97**, 6264 (2000).
- [18] J.M. Heller, Jr. *et al.*, *J. Chem. Phys.* **60**, 3483 (1974).
- [19] R. Onaka and T. Takahashi, *J. Phys. Soc. Jpn.* **24**, 548 (1968).
- [20] G.P. Parravicini and L. Resca, *Phys. Rev. B* **8**, 3009 (1973).
- [21] B.D. Bursulaya, J. Jeon, C.-N. Yang, and H.J. Kim, *J. Phys. Chem. A* **104**, 45 (2000).
- [22] P.H. Hahn *et al.*, *Phys. Rev. Lett.* **94**, 037404 (2005).
- [23] P. Pruzan, J.C. Chervin, and B. Canny, *J. Chem. Phys.* **99**, 9842 (1993).
- [24] M. Benoit, D. Marx, and M. Parrinello, *Nature (London)* **392**, 258 (1998).
- [25] P. Loubeyre *et al.*, *Nature (London)* **397**, 503 (1999).
- [26] M. Benoit, A.H. Romero, and D. Marx, *Phys. Rev. Lett.* **89**, 145501 (2002).
- [27] R. Caracas, *Phys. Rev. Lett.* **101**, 085502 (2008).
- [28] B. Militzer and H.F. Wilson, *Phys. Rev. Lett.* **105**, 195701 (2010).
- [29] G. Kresse and J. Furthmüller, *Phys. Rev. B* **54**, 11 169 (1996).
- [30] D. Vanderbilt, *Phys. Rev. B* **41**, R7892 (1990).
- [31] H.J. Monkhorst and J.D. Pack, *Phys. Rev. B* **13**, 5188 (1976).
- [32] J.P. Perdew *et al.*, *Phys. Rev. B* **46**, 6671 (1992).
- [33] L. Hedin, *Phys. Rev.* **139**, A796 (1965).
- [34] G. Onida, L. Reining, and A. Rubio, *Rev. Mod. Phys.* **74**, 601 (2002).
- [35] W.G. Schmidt *et al.*, *Phys. Rev. B* **67**, 085307 (2003).
- [36] V. Garbuio *et al.*, *Phys. Rev. Lett.* **97**, 137402 (2006).
- [37] F. Bechstedt *et al.*, *Solid State Commun.* **84**, 765 (1992).
- [38] M. Shishkin, M. Marsman, and G. Kresse, *Phys. Rev. Lett.* **99**, 246403 (2007).
- [39] A.J. Leadbetter *et al.*, *J. Chem. Phys.* **82**, 424 (1985).
- [40] B. Kamb *et al.*, *J. Chem. Phys.* **55**, 1934 (1971).
- [41] W.F. Kuhs *et al.*, *J. Chem. Phys.* **81**, 3612 (1984).
- [42] J.M. Besson *et al.*, *Phys. Rev. B* **49**, 12 540 (1994).
- [43] E. Whalley, *Trans. Faraday Soc.* **53**, 1578 (1957).
- [44] P.H. Gammon, H. Kiefte, and M.J. Clouter, *J. Phys. Chem.* **87**, 4025 (1983).
- [45] A. Hermann and P. Schwerdtfeger, *Phys. Rev. Lett.* **101**, 183005 (2008).
- [46] H. Stoll, *Phys. Rev. B* **46**, 6700 (1992).
- [47] H. Nakatsuji, *Chem. Phys. Lett.* **59**, 362 (1978).
- [48] H. Nakatsuji, *Chem. Phys. Lett.* **67**, 334 (1979).
- [49] M.J. Frisch *et al.*, *Gaussian 03, Revision C.02* (Gaussian, Inc., Wallingford, CT, 2004).
- [50] E.R. Batista, S.S. Xantheas, and H. Jónsson, *J. Chem. Phys.* **109**, 4546 (1998).
- [51] P.L. Silvestrelli and M. Parrinello, *Phys. Rev. Lett.* **82**, 3308 (1999).